Efficient Solution for System Frequency Security-Constrained Optimization via Combined Smooth Approximation and Trajectory Sensitivity

Shuaishuai Feng[1], Deping Ke[1], Xiaojie Pan[2], Jian Xu[1], Siyang Liao[1]
1. School of Electrical Engineering and Automation, Wuhan University, Wuhan 430072, China
2. Central China Branch, State Grid Corporation of China, Wuhan 430070, China

***Abstract*—Optimization problems with system frequency-security constraints often suffer from inaccurate gradient evaluations, thereby degrading the solution efficiency. The inaccuracies mainly arise from non-analytic sequential time-step iterations about frequency dynamics and the presence of non-differentiable components, such as saturation limits. This paper proposes a simple yet sufficiently accurate smooth approximation method for replacing some typical non-differentiable components in power systems, using a truncated Fourier-series formulation. Furthermore, an efficient calculation scheme for system frequency-constraint gradients is developed based on trajectory sensitivity analysis, enabling efficient solution for optimization with embedded frequency-security constraints. The effectiveness of the proposed method is validated through simulations of the emergency frequency control optimization problem on an actual regional power system.**

***Keywords*—Frequency-constrained optimization, gradient calculation, smooth approximation, trajectory sensitivity, efficient solution.**

I. INTRODUCTION

During power system operation and control, frequency-security-constrained optimization problems are routinely involved, including operating-boundary evaluation, economic dispatch, emergency frequency control (EFC) and so on [1]. For example, in direct current (DC) sending-end grids with high renewable penetration, a DC transmission blocking fault can cause a sharp system frequency rise. To mitigate this risk, an EFC strategy must be pre-generated and activated immediately upon fault detection. Recent studies also investigate replacing conventional generator tripping with rapid power curtailment of photovoltaics (PVs) and wind turbines (WTs) to reduce control costs [2]. In such cases, the pre-generation of WT and PV control orders is equivalent to solving an EFC-related frequency-constrained optimization problem. Moreover, frequent changes in system operation states, caused by large-scale renewable integration, require this optimization to be executed efficiently. This enables periodic updates of the pre-generated control orders according to the monitored operating states.

However, solving such frequency-constrained optimization problems efficiently remains challenging due to the nonlinear and non-analytical calculation of post-event frequency dynamics. The dynamics are typically analyzed by electromechanical simulation or numerical integration on sufficiently detailed system frequency response (SFR) models [3]. Some data-driven approaches have also been introduced to simulate system frequency well, but their performance often relies on data quality, lack physical interpretability, and typically require retraining when operation scenarios change [4]. In many cases, the trained models further act as black boxes or highly nonlinear components within the optimization framework. For this class of optimization problems, where the underlying models are complex, nonlinear and non-analytical, existing solution methods fall into two categories: gradient-free heuristic algorithms and gradient-based methods. Heuristic algorithms avoid explicit gradient computation. However, each iteration requires multiple evaluations of the objective and constraints to infer a search direction, which effectively approximates the gradient through multi-point comparisons. Gradient-based methods cannot directly oabtain an analytical gradient for such frequency-constrained problems, and therefore rely on finite-difference or perturbation techniques [5]. These techniques are sensitive to step size, prone to numerically instability, and compute gradients with respect to only one variable at a time. Moreover, since frequency-related constraints necessitate sequential time-step iterations, both heuristic and gradient-based methods suffer from low computational efficiency when emulating gradients.

In addition, non-differentiable components in power systems, such as saturation limiters, amplifies numerical instability in finite-difference gradient calculations, thereby hindering optimization processes. To handle gradients at non-differentiable points, several methods have been proposed, including the sub-gradient method, smooth approximation, and kernel-based convolution. The sub-gradient method randomly selects a gradient near the non-differentiable point [6], which introduces discontinuity, slowing convergence and providing no second-order information such as the Hessian. Kernel-based methods smooth non-differentiable points through convolution, but their performance strongly depends on the kernel choice and parameters. And the results are typically numerical without a simple analytical form [7]. Existing smooth approximation techniques often compromise local accuracy near non-differentiable points to improve overall performance, which may lead to undesirable results [8].

Therefore, considering the frequency-constrained optimization problem of coordinating WT and PV power curtailment for EFC as the research scenario, this paper proposes an efficient method for calculating system frequency-constraint gradients, driven jointly by a Fourier series–based smooth approximation and trajectory sensitivity analysis. The main contributions are as follows:

(1) A Fourier series-based smoothing method is proposed to accurately approximate typical non-differentiable components in power systems.

This work was supported the science and technology project of Central China Branch of State Grid Corporation of China (521400250003).
(*Corresponding author: Deping Ke, kedeping@whu.edu.cn*)
979-8-3315-8138-1

(2) A frequency-constraint gradient calculation method combing the smooth approximation with trajectory sensitivity analysis is developed, enabling efficient solution for frequency-security-constrained optimization problems in power systems.

II. Smooth Approximation of Typical Non-Differentiable Components

A. Fundamentals of system frequency security-constrained emergency control

A system frequency response model is constructed to characterize the system frequency dynamics under the coordinated control of WTs and PVs, as presented in Fig. 1.

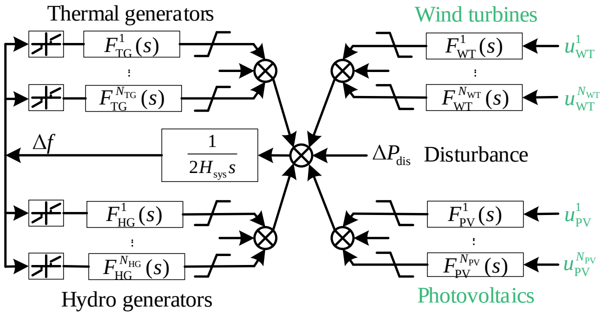

Fig. 1. System frequency response model incorporating WT and PV control.

$F_{\mathrm{TG}}^{i}(s)$ and $F_{\mathrm{HG}}^{j}(s)$ are formulated as transfer functions that capture the primary frequency-regulation dynamics of conventional generators. $F_{\mathrm{PV}}^{m}(s)$ is modeled as a first-order inertial block with a small time constant to describe the dynamic response of PV power curtailment. To enable low-cost WT power reduction, the rotor kinetic energy control is adopted in this paper. An auxiliary control order u_{WT} is added after the torque-control loop to enforce a rapid decrease in WT output, mitigating the transient frequency rise. The output then gradually returns to its initial value. The simplified power control model is illustrated in Fig. 2.

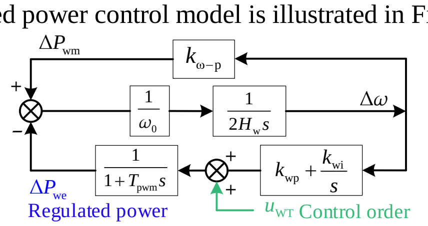

Fig. 2. Simplified active power control structure of wind turbine.

where, H_{w} represents the inertia constant of the WT rotor, ω_0 denotes the initial rotor speed. The parameters k_{wp}, k_{wi} and $k_{\omega-\mathrm{p}}$ are constant coefficients. Due to the fast-dynamic response of the inverter-side PWM modulation, it is modeled as a first-order inertial block with time constant T_{pwm}. The variable ΔP_{wm} and ΔP_{we} denote the mechanical power deviation and the power regulation. Under this formulation, the overall system is described by the transfer function $F_{\mathrm{WT}}^{m}(s)$, which maps the control input u_{wt} to the output ΔP_{we}.

B. Optimization model formulation

Considering the predefined large disturbance ΔP_{dis} in Fig.1, the power-reduction orders u_{WT} and u_{PV} must be optimized and pre-generated, to ensure immediate dispatch upon fault occurrence. Accordingly, an optimization model for the EFC strategy is established to minimize the total control costs while enforcing system frequency security and transmission-line thermal constraints, as formulated below:

$$\min\ C_{\mathrm{EFC}}=\sum_{m=1}^{N_{\mathrm{wt}}}-C_{\mathrm{wt}}^{m}\times u_{\mathrm{wt}}^{m}\times S_{\mathrm{wt}}^{m}+\sum_{n=1}^{N_{\mathrm{pv}}}-C_{\mathrm{pv}}^{n}\times u_{\mathrm{pv}}^{n}\times S_{\mathrm{pv}}^{n} \tag{1}$$

$$f_{\mathrm{m}}\le f_{\mathrm{m}}^{\mathrm{up}} \tag{2}$$

$$f_{\mathrm{res}}\le f_{\mathrm{res}}^{\mathrm{up}} \tag{3}$$

$$\left|P_{ij}\right|\le P_{ij}^{\mathrm{up}},\ \forall i-j\in\Omega_{\mathrm{Lines}} \tag{4}$$

where, u_{wt} and u_{pv} are the decision variables; C_{EFC} represents the total control cost; S_{wt} and S_{pv} denote the rated capacities of WTs and PVs; C_{wt} and C_{pv} denote their unit control costs; f_{m} and f_{res} denote the maximum and steady-state value of the post-event system frequency, and their security limits are given by $f_{\mathrm{m}}^{\mathrm{up}}$ and $f_{\mathrm{res}}^{\mathrm{up}}$. P_{ij} denotes the transmission power on the line from bus i to bus j, and P_{ij}^{up} is its transmission limit. Ω_{Lines} denotes the set of critical transmission lines.

The system frequency in (2) and (3) is obtained by applying decision variables u_{wt} and u_{pv} to the model in Fig. 1 and performing numerical integration. Meanwhile, the output power dynamics of photovoltaics and wind turbines are also derived. Further, the power injection variation $\Delta P_i^{\mathrm{inj}}$ at bus i is defined as the sum of the steady-state power adjustments of all photovoltaics $\Delta P_p^{\mathrm{inj.pv}}$ and generators $\Delta P_g^{\mathrm{inj.cg}}$ connected to that bus. Based on these, the corresponding line power flows are then evaluated using the DC power flow model, expressed as:

$$\Delta P_i^{\mathrm{inj}}=\sum_{g\in\mathcal{G}_i}\Delta P_g^{\mathrm{inj.cg}}+\sum_{p\in\mathcal{P}_i}\Delta P_p^{\mathrm{inj.pv}} \tag{5}$$

$$\boldsymbol{P}^{\mathrm{inj}}=\boldsymbol{P}_0^{\mathrm{inj}}+\Delta\boldsymbol{P}^{\mathrm{inj}},\ \boldsymbol{\theta}=\boldsymbol{B}^{-1}\boldsymbol{P}^{\mathrm{inj}},\ P_{ij}=(\theta_i-\theta_j)\times B_{ij} \tag{6}$$

where, $\mathcal{G}_i$ and $\mathcal{P}_i$ denote the conventional generators and photovoltaics connected to bus i, respectively. $\boldsymbol{P}_0^{\mathrm{inj}}$, $\Delta\boldsymbol{P}^{\mathrm{inj}}$ and $\boldsymbol{P}^{\mathrm{inj}}$ denote the matrices of the initial, the regulated, and the post-event injected power at all bus nodes. $\boldsymbol{\theta}$ denotes the bus voltage angles, including θ_i and θ_j, while $\boldsymbol{B}$ represents the admittance matrix, with B_{ij} indicating the admittance between buses i and j.

C. Fourier series–based smooth approximation method

The saturation limiter is typically modeled as a piecewise function, as shown in Fig. 3(a). In practice, the variable x (in Fig. 3) operates within a normal range $[0,x_{\mathrm{nom}}^{\mathrm{up}}]$, rather than being unbounded. For example, the power or current of equipment is inherently bounded by its capacity constraints. Therefore, the key requirement of the smooth approximation is to maintain high fidelity within the normal range $[0,x_{\mathrm{nom}}^{\mathrm{up}}]$.

Subsequently, a Fourier series-based approximation is proposed to obtain a smooth representation. Firstly, the original function on the interval $[0,x_{\mathrm{nom}}^{\mathrm{up}}]$ is extended periodically to enable its Fourier-series approximation. The resulting periodic function is shown in Fig. 3(b), and its standard Fourier series form is expressed as follows:

$$f_{\mathrm{lmt}}^{\mathrm{b}}(x)\sim F_{\mathrm{lmt}}^{\mathrm{b}}(x)=a_0+\sum_{n=1}^{\infty}\left[a_n\cos(nx)+b_n\sin(nx)\right] \tag{7}$$

where, a_0, b_n, and c_n(n=1,2,3,...) are constant coefficients computed based on the function $f_{\mathrm{lmt}}^{\mathrm{b}}$. In particular, the Fourier expansion of a half-wave symmetric function has a simplified structure, as it contains only odd-order cosine terms. Accordingly, to enhance approximation accuracy while reducing the complexity of series expansion, the structural properties of the function $f_{\mathrm{lmt}}^{\mathrm{b}}$ in Fig. 3(b) are modified without altering its output characteristics within $[0, x_{\mathrm{nom}}^{\mathrm{up}}]$. Specifically, the function is transformed to possess both half-wave symmetry and odd symmetry about the origin. As illustrated in Fig. 3, the function $f_{\mathrm{lmt}}^{\mathrm{b}}$ is first extended to form an axially symmetric periodic function $f_{\mathrm{lmt}}^{\mathrm{c}}$. It is then converted into an origin-symmetric form, with the resulting function $f_{\mathrm{lmt}}^{\mathrm{d}}$ serving as the basis for the Fourier series expansion. Finally, the approximation is derived as follows:

$$f_{\mathrm{lmt}}^{\mathrm{d}}(x) \sim F_{\mathrm{lmt}}^{\mathrm{d}}(x) \approx \sum_{n=1}^{N_{\mathrm{FS}}} b_n \sin(n\omega t),\ n = 1,3,5... \tag{8}$$

$$b_n = \frac{4}{T} \times \frac{\sin(n\omega\alpha) + \sin\left(n\omega x_{\mathrm{nom}}^{\mathrm{up}}\right) - \sin\left[n\omega(\alpha + x_{\mathrm{nom}}^{\mathrm{up}})\right]}{(n\omega)^2} \tag{9}$$

where, $\omega = 2\pi / T$, $T = 2 \times (x_{\mathrm{nom}}^{\mathrm{up}} + \alpha)$. α denotes the saturation value; N_{FS} denotes the truncation order. Subsequent tests indicate that setting N_{FS}=10 can yield a highly accurate approximation of the saturation limiter. In other words, only five sine terms are enough, confirming the effectiveness of the simplification in Fig. 3.

Additionally, this paper also proposes a smooth approximation method for the dead-band characteristic in power systems, expressed as:

$$\begin{aligned} f_{\mathrm{db}}(x) = &\left[\frac{L_{\mathrm{th}}}{2} \times \left(\tanh\left(s_{\mathrm{tan}} \times \left(x - L_{\mathrm{th}}\right)\right) + 1\right)\right] \\ &+ \left[\frac{1}{2 s_{\mathrm{ln}}} \ln\left(\cosh(s_{\mathrm{ln}} \times (x - L_{\mathrm{th}}))\right) + \frac{1}{2}\left(x - L_{\mathrm{th}}\right)\right] \end{aligned} \tag{10}$$

where, s_{ln} represents the constant scaling factor, and L_{th} denotes the translation length. This smooth approximation is obtained by combining a scaled and shifted hyperbolic tangent function tanh(x), a hyperbolic cosine function cosh(x), and a linear term.

III. Gradient Calculation of Frequency Constraints via Trajectory Sensitivity

A. Numerical evaluation of system frequency dynamics

The SFR model in Fig. 1 can be converted into its state-space representation, by the canonical form method [9]. Non-differentiable components are accurately represented through smooth approximation. As a result, the model can be systematically expressed in the following standard form:

$$\begin{cases} \dot{\boldsymbol{x}}_{\mathrm{f}}(t) = \boldsymbol{f}_{\mathrm{f}}\left(\boldsymbol{x}_{\mathrm{f}}(t), \boldsymbol{u}_{\mathrm{f}}\right) \\ \boldsymbol{0} = \boldsymbol{g}_{\mathrm{f}}\left(\boldsymbol{x}_{\mathrm{f}}(t), \boldsymbol{u}_{\mathrm{f}}(t)\right) \end{cases} \tag{11}$$

where, $\boldsymbol{f}_{\mathrm{f}}$ and $\boldsymbol{g}_{\mathrm{f}}$ represent the functions defining the state and output equations, respectively. The term $\boldsymbol{u}_{\mathrm{f}}$ represents the time-invariant control input, corresponding to the decision variables u_{WT} and u_{PV} in Fig. 1. The variables $\boldsymbol{x}_{\mathrm{f}}$ and $\boldsymbol{y}_{\mathrm{f}}$ represent the state and algebraic variables, respectively. And the system frequency f is explicitly included as one of the state variables.

Thus, evaluating the system frequency dynamics requires computing the time-domain trajectory of $\boldsymbol{x}_{\mathrm{f}}$. This study employs the trapezoidal integration method to calculate it

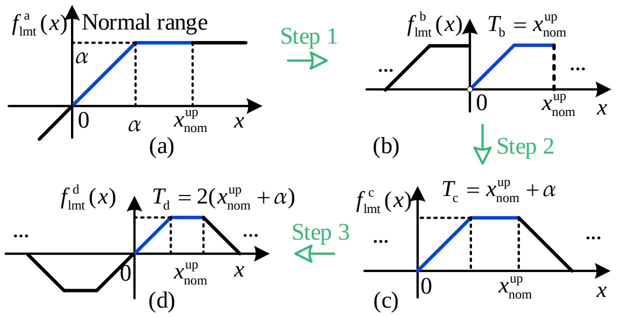

Fig. 3. The process of smooth approximation about the saturation limiter.

based on (11), as follows:

$$\boldsymbol{x}_{\mathrm{f}}(t_2) = \boldsymbol{x}_{\mathrm{f}}(t_1) + \frac{\dot{\boldsymbol{x}}_{\mathrm{f}}(t_1) + \dot{\boldsymbol{x}}_{\mathrm{f}}(t_2)}{2} \times \Delta T \tag{12}$$

where, ΔT denotes the time step and t_2=t_1+ΔT. Substituting the state equation in (11) into (12) yields:

$$\overbrace{\boldsymbol{x}_{\mathrm{f}}(t_2) - \frac{\Delta T}{2} \times \boldsymbol{f}_{\mathrm{f}}\left(\boldsymbol{x}_{\mathrm{f}}(t_2), \boldsymbol{u}_{\mathrm{f}}(t_2)\right)}^{\text{Unknown}} - \overbrace{\left[\boldsymbol{x}_{\mathrm{f}}(t_1) + \frac{\Delta T}{2} \times \boldsymbol{f}_{\mathrm{f}}\left(\boldsymbol{x}_{\mathrm{f}}(t_1), \boldsymbol{u}_{\mathrm{f}}(t_1)\right)\right]}^{\text{Known}} = 0 \tag{13}$$

Equation (13) defines a system of equations with respect to the the variable $\boldsymbol{x}_{\mathrm{f}}(t_2)$. The system can be solved using the Newton method, for details in [9]. Consequently, the value of $\boldsymbol{x}_{\mathrm{f}}(t_2)$ is derived from $\boldsymbol{x}_{\mathrm{f}}(t_1)$.

Following this procedure, the system frequency dynamics (including the maximum and steady-state values) are computed though the above sequential time-step iterations.

B. Gradient calculation based on trajectory sensitivity

Based on the model in (11), trajectory sensitivity analysis is employed to evaluate the gradient of the system frequency constraint with respect to the control inputs. Trajectory sensitivity characterizes how perturbations in system inputs or parameters influence any point along the system frequency trajectory. To obtain this sensitivity, the partial derivative of (11) with respect to the control input $\boldsymbol{u}_{\mathrm{f}}$ is taken, as follows [10]:

$$\frac{d}{dt}\left(\frac{\partial \boldsymbol{x}_{\mathrm{f}}(t)}{\partial \boldsymbol{u}_{\mathrm{f}}}\right) = \frac{\partial \boldsymbol{f}}{\partial \boldsymbol{x}_{\mathrm{f}}}\left(\boldsymbol{x}_{\mathrm{f}}(t), \boldsymbol{u}_{\mathrm{f}}\right) \times \frac{\partial \boldsymbol{x}_{\mathrm{f}}(t)}{\partial \boldsymbol{u}_{\mathrm{f}}} + \frac{\partial \boldsymbol{f}}{\partial \boldsymbol{u}_{\mathrm{f}}}\left(\boldsymbol{x}_{\mathrm{f}}(t), \boldsymbol{u}_{\mathrm{f}}\right) \tag{14}$$

where, $\partial \boldsymbol{x}_{\mathrm{f}} / \partial \boldsymbol{u}_{\mathrm{f}}$ is defined as the trajectory sensitivity of $\boldsymbol{x}_{\mathrm{f}}$ with respect to $\boldsymbol{u}_{\mathrm{f}}$, and is denoted as $\boldsymbol{x}_{\mathrm{f}}|\boldsymbol{u}_{\mathrm{f}}$ in this paper. At the operating point specified by $\boldsymbol{u}_{\mathrm{f}}$=$\boldsymbol{u}_{\mathrm{f0}}$, (12) can be rewritten in a state-space form by introducing $\boldsymbol{S}$=$\boldsymbol{x}_{\mathrm{f}}|\boldsymbol{u}_{\mathrm{f}}$ as the new state variable, as follows:

$$\dot{\boldsymbol{S}}(t) = \boldsymbol{L}(t) \times \boldsymbol{S}(t),\ \boldsymbol{L}(t) = \frac{\partial \boldsymbol{f}}{\partial \boldsymbol{x}_{\mathrm{f}}}\left(\boldsymbol{x}_{\mathrm{f}}(t), \boldsymbol{u}_{\mathrm{f}}\right)\Big|_{u_{\mathrm{f}} = u_{\mathrm{f0}}} \tag{15}$$

Since $\boldsymbol{x}_{\mathrm{f}}(t)$ is obtained during the frequency calculation in (11)-(13), the sequence $\boldsymbol{L}$ is known a priori. With the coefficient $\boldsymbol{L}$ available, the trajectory sensitivity $\boldsymbol{S}$=$\boldsymbol{x}_{\mathrm{f}}|\boldsymbol{u}_{\mathrm{f}}$ can be computed following the procedure (11)-(13). The gradient $f_{\mathrm{m}}|\boldsymbol{u}_{\mathrm{f}}$ of the maximum-frequency constraint is then naturally determined by the value of trajectory $\boldsymbol{x}_{\mathrm{f}}|\boldsymbol{u}_{\mathrm{f}}$ at the time instant when the maximum frequency occurs.

Notably, since $\boldsymbol{u}_{\mathrm{f}}$ is defined as a vector comprising all control orders, $\boldsymbol{x}_{\mathrm{f}}|\boldsymbol{u}_{\mathrm{f}}$ represents the sensitivity matrix about these orders. Consequently, all gradients can be computed in a single step through matrix operations, as outlined in (15). This method is significantly more efficient than the finite-difference approach, which necessitates an individual perturbation for each gradient calculation.

In practice, the hybrid system approach is typically adopted for trajectory sensitivity analysis in systems with non-differentiable points. This method performs piecewise analysis at each non-differentiable point, requiring additional computations about both the sensitivities of the switching time t_{sw} and variables $\boldsymbol{x}_f$ (t_{sw}) with respect to $\boldsymbol{u}_f$ [11]. While trajectories frequently encounter non-differentiable points, the method suffers from reduced numerical stability and increased computational cost. In contrast, applying the proposed smooth approximation for system modeling in (11) can effectively avoid these issues.

IV. Case Study

A. System introduction

To validate the effectiveness of the proposed method, a case study is presented on pre-generation of the optimal EFC strategy for an actual regional power system, as shown in Fig. 4. This is a DC sending-end system characterized by a high penetration of wind and photovoltaic generation, comprising 19 wind farms (represented as WTs) and 27 PV units. The simulations investigate frequency-rising events resulting from the potential bipolar DC blocking fault near Bus 10, featuring a transmission capacity of 8000 MW. The proposed method is employed to rapidly solve the corresponding optimization problem for EFC strategies, leveraging coordinated regulation of WTs and PVs. Here, system frequency security is enforced by the upper limits $f_m^{up} = 50.5\text{Hz}$ and $f_{res}^{up} = 50.2\text{Hz}$. The time-step size used for numerical integration to simulate the system-frequency dynamics is set to 0.02 s.

B. Accuracy of the proposed smooth approximation

This paper proposes a Fourier series (FS)–based method for the smooth approximation of saturation limiters. Its performance is evaluated against three existing methods: (1) using hyperbolic tangent (HT) functions: $y_{tan}=U_{max}\tanh(k_{tanh}x)$; (2) using regularization-based (RG) functions: $y_{rg}=U_{max}x/\sqrt{x^2+\varepsilon_{rg}}$; (3) convolution with kernel (CK) functions. Using an amplitude limit of U_{max}=0.5 as an example, Fig. 5 compares the smooth approximations produced by these methods. With only five sine terms, the proposed FS-based method closely matches the original function, demonstrating superior approximation accuracy. A smoothing approximation of the dead-zone nonlinearity is also presented, and its effectiveness is illustrated in Fig. 5(b).

C. Presentation of solution efficiency

This subsection defines three comparative scenarios, each reflecting a distinct solution strategy, to systematically evaluate the effectiveness of the proposed method: (1) Case I-Proposed analytical gradient-decent method: Implements the developed smooth approximation in conjunction with trajectory sensitivity; (2) Case II-Standard gradient-decent method: Computes frequency-constraint gradients using the finite difference method [5]. For example,

$$f_m \mid u_{WT}^i = \frac{f_m\left\langle u_0^i + h\right\rangle - f_m\left\langle u_0^i\right\rangle}{h}, \tag{16}$$

where h is the step size, and $f_m < u_0^i >$ denotes the maximum frequency f_m under the condition $u_{WT}^i = u_0^i$; (3) Case III-Heuristic algorithm: A gradient-free optimization approach.

For Case I, a multi-start search strategy is applied. The

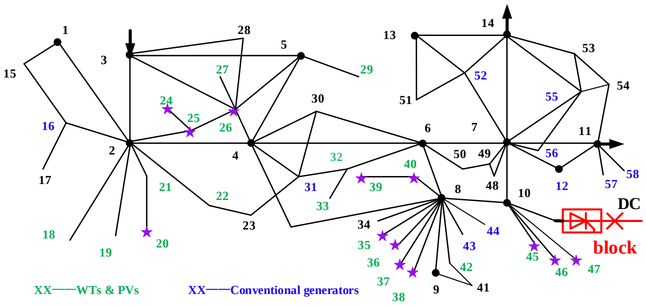

Fig. 4. The simplified topology of the simulation system.

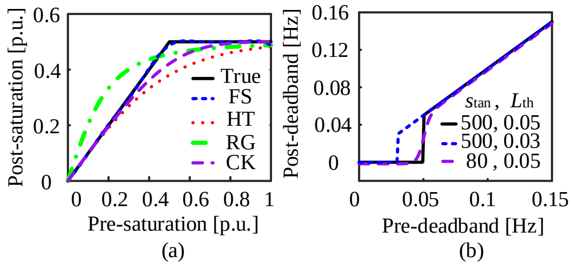

Fig. 5. Smooth approximation effects of: (a) saturation limiter; (b) dead band

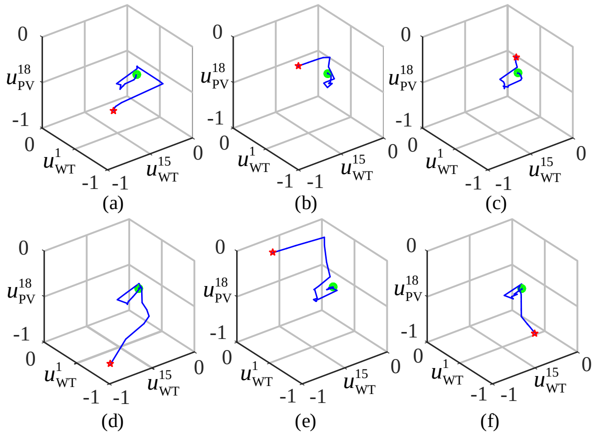

Fig. 6. Search results under different initial conditions in Case I.

results in Fig. 6 indicate that the optimization converges to a local neighborhood. To improve visualization, the three decision variables u_{WT}^1, u_{WT}^{15}, and u_{PV}^{18} are plotted in per-unit form and used as spatial coordinates. In Fig.4, the PVs and WTs with significant power regulation are marked with star symbols. These units are mainly concentrated around Bus 10 and Bus 8 near the DC transmission system, constrained by the transmission power limits in (4). The active-power regulation responses of these units, represented by WT_1 and PV_{18}, are shown in Fig. 7(c). Fig. 7(a) gives the post-event system frequency, which fully satisfies the security requirement. The primary-frequency regulation response of conventional units is presented in Fig. 7(b). As visible in the inset, the dead band introduces a delayed activation of power regulation. To illustrate the gradient calculation, Fig. 7(d) plots the trajectory-sensitivity (TS) curves of system frequency dynamics with respect to orders u_{WT}^1 and u_{WT}^{18}. And the gradient of the maximum-frequency constraint with respect to u_{WT}^1 equals the value of the TS curve at the time of the maximum frequency observed in Fig. 7(a).

Accordingly, gradients are evaluated at each iteration to guide the optimization process. Fig. 8(b) presents gradients of the constraint f_m with respect to u_{WT}^1, along with the convergence curve obtained in Case I, which terminates after 37 iterations. For comparison, Fig. 8(a) reports the

979-8-3315-8138-1

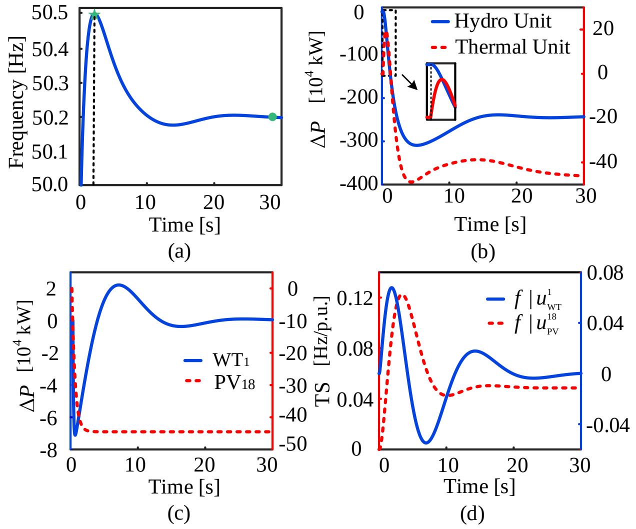

Fig. 7. Control performance of the optimal strategies: (a) system frequency; (b) power response of the conventional generators; (c) power regulation of PV and WT; (d) trajectory sensitivity of frequency about control orders.

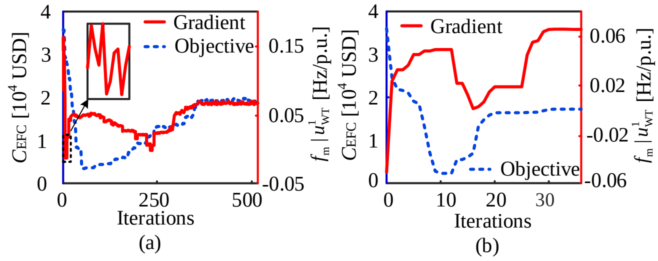

Fig. 8. Optimization convergence curves and constraint gradients during search process of: (a) case 2; (b) case 1.

corresponding gradient information and convergence trajectory, where 531 iterations are required. The finite difference method is step-size sensitive and suffers from poor numerical stability, which causes persistent fluctuations in computed gradients. The accumulated errors in multivariable gradient evaluations lead to a significant deviation from the true steepest-descent direction. Consequently, the convergence slows down and the number of iterations increases. It is worth noting that all tests employ a standard gradient-based interior-point method. As a result, the convergence curves exhibit an initial decrease followed by a slight increase, indicating that early iterations may generate search points that temporarily violate the underlying constraints.

Especially near non-differentiable regions, the computed gradient becomes highly sensitivity to the selected step size. The combined influence of differential step-size variation and the time shift of the maximum-frequency instant leads to substantial fluctuations in the computed gradient, as highlighted in the inset of Fig. 8(a). In contrast, Case I employs the analytic gradient based on smooth approximation, which yields significantly more stable results, as shown in Fig. 8 (b).

Case III, which employs heuristic algorithms, is also evaluated, and the results for all three cases are summarized in Table I. The solution time of Case II is significantly longer than Case I, and this increase is not proportional to iterations. This primary reason lies in the different gradient-evaluation method. As indicated in (15), Case I computes the gradients of all variables in a single batch at each iteration, whereas this is not feasible for Case II. Case III

TABLE I: PERFORMANCE OF DIFFERENT METHODS IN THE THREE CASES

Case	Case I	Case II	Case III
Solution time (s)	4	217	133
Control costs (USD)	17 835	19 150	18 365

also incurs high computational cost because each iteration requires evaluating constraint information across numerous data points. It is worth noting that Case I achieves the lowest control cost among the three cases, owing to its more accurate and reliable gradient computation. The proposed efficient solution method better accommodates the practical "offline computation–online matching" framework, enabling emergency control strategies to be updated at a minute-level (5-15 min) timescale required in engineering practice.

V. CONCLUSION

This paper proposes a novel Fourier series–based smooth approximation method to address typical non-differentiable components in power systems. Additionally, an efficient trajectory sensitivity-based gradient calculation scheme for system frequency-security constraints is developed, accelerating the solution of optimization problems subject to system frequency-security constraints. Its effectiveness is demonstrated through case studies about pre-generating emergency frequency control strategies on an actual regional power system. Results show that the proposed method achieves significantly faster solution times compared with conventional approaches.

REFERENCES

[1] H. Zhao, X. Yang, T. Hong, B. Zhang, and Y. Wang, "Modeling of frequency security constraints and quantification of frequency control reserve capacities for unit commitment," *IEEE Trans. Power Syst.*, vol. 39, no. 1, pp. 297-310, Jan. 2024.

[2] C. Ye, K. Jiang, D. Liu, "Emergency control strategy for high proportion renewable power system considering the frequency aggregation response of multi-type power generations," in *IEEE Access*, vol. 12, pp. 188325-188335, 2024,

[3] Q. Shi, F. F. Li, "Analytical method to aggregate multi-machine sfr model with applications in power system dynamic studies," in *IEEE Trans. Power Syst.*, vol. 33, no. 5, pp. 5440-5448, Sep. 2018.

[4] M. Jalali, V. Kekatos, S. Bhela, "Inferring power system dynamics from synchrophasor data using gaussian processes," in *IEEE Trans. Power Syst.*, vol. 37, no. 6, pp. 4409-4423, Nov. 2022

[5] M. -B. Radac and T. Nicolae, "Leveraging simplex gradient variance and bias reduction for black-box optimization of noisy and costly functions," in *IEEE Access*, vol. 13, pp. 14304-14316, 2025

[6] T. Tong, "Low-rank matrix recovery with scaled subgradient methods: fast and robust convergence without the condition number," in *IEEE Trans. Signal Process.*, vol. 69, pp. 2396-2409, 2021.

[7] W. Yang et al., "Smooth multiple kernel K-means via underlying graph filtering," in *IEEE Trans. Neural Netw. Learn. Syst.*, vol. 36, no. 8, pp. 14855-14868, Aug. 2025

[8] A. D. Roshan, P. Guha and G. Trivedi, "Hardware-optimized regression tree-based sigmoid and tanh functions for machine learning applications," in *IEEE Trans. Circuits Syst. II, Express Briefs*, vol. 72, no. 1, pp. 283-287, Jan. 2025

[9] R. C. Dorf and R. H. Bishop, Modern control systems, 13th ed. Upper Saddle River, NJ, USA: *Pearson Education*, 2016.

[10] R. Nagi, X. Huan and Y. C. Chen, "Bayesian inference of parameters in power system dynamic models using trajectory sensitivities," in *IEEE Trans. Power Syst.*, vol. 37, no. 2, pp. 1253-1263, March 2022.

[11] I. A. Hiskens and M. A. Pai, "Trajectory sensitivity analysis of hybrid systems," in *IEEE Trans. Circuits Syst. I, Fundam. Theory Appl.*, vol. 47, no. 2, pp. 204-220, Feb. 2000.